Y.-W. Lin, S.-S. Li, Z. Ren, and C. T.-C. Nguyen, "Vibrating micromechanical resonators with solid dielectric capacitive-transducer 'gaps'," *Proceedings*, Joint IEEE Int. Frequency Control/Precision Time & Time Interval Symposium, Vancouver, Canada, Aug. 29-31, 2005, pp. 128-134. ***(best paper award winner)***

Vibrating Micromechanical Resonators With Solid Dielectric Capacitive Transducer Gaps

Yu-Wei Lin, Sheng-Shian Li, Yuan Xie, Zeying Ren, and Clark T.-C. Nguyen
Center for Wireless Integrated Micro Systems
Department of Electrical Engineering and Computer Science
University of Michigan, Ann Arbor, Michigan 48109-2122, USA

***Abstract*—VHF and UHF MEMS-based vibrating micromechanical resonators equipped with new solid dielectric (i.e., filled) capacitive transducer gaps to replace previously used air gaps have been demonstrated at 160 MHz, with *Q*'s ~ 20,200 on par with those of air-gap resonators, and motional resistances (R_x's) more than 8× smaller at similar frequencies and bias conditions. This degree of motional resistance reduction comes about via not only the higher dielectric constant provided by a solid-filled electrode-to-resonator gap, but also by the ability to achieve smaller solid gaps than air gaps. These advantages with the right dielectric material may now allow capacitively-transduced resonators to match to the 50-377 Ω impedances expected by off-chip components (e.g., antennas) in many wireless applications without the need for high voltages. In addition to lower motional resistance, the use of filled-dielectric transducer gaps provides numerous other benefits over the air gap variety, since it (a) better stabilizes the resonator structure against shock and microphonics; (b) eliminates the possibility of particles getting into an electrode-to-resonator air gap, which poses a potential reliability issue; (c) greatly improves fabrication yield, by eliminating the difficult sacrificial release step needed for air gap devices; and (d) potentially allows larger micromechanical circuits (e.g., bandpass filters comprised of interlinked resonators) by stabilizing constituent resonators as the circuits they comprise grow in complexity.**

***Keywords*—MEMS, micromechanical, capacitive transducer, resonator, high quality factor, motional resistance, fabrication yield.**

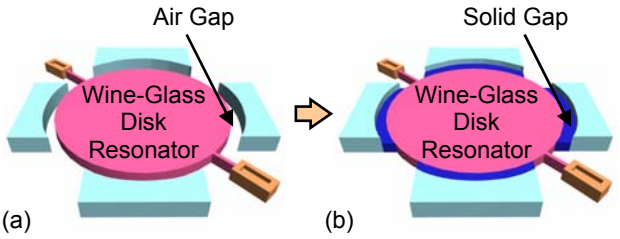

Fig. 1: Perspective-view schematics comparing an air-gap micromechanical wine-glass disk resonator with the solid-gap variety used in this work.

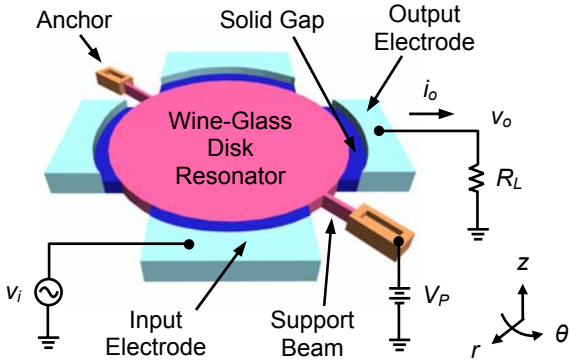

Fig. 2: Perspective-view schematic of a solid-gap micromechanical wine-glass disk resonator in two-port bias, drive, and sense configuration.

I. Introduction

Capacitively transduced vibrating micromechanical resonators have recently been demonstrated with resonant frequencies in the GHz range with *Q*'s still larger than 11,000 [1][2][3], making them very attractive as on-chip frequency control elements for oscillators and filters in wireless communications. Although solutions now exist to many of the issues that once hindered deployment of these devices in RF front ends [4], including aging [5][6] and temperature stability [7], the need for high bias voltages to reduce impedances, especially in the VHF and UHF ranges, still remains a troublesome drawback of this technology. For example, in reference oscillator applications, where the impedance of the micromechanical resonator must be low enough to allow oscillation startup, dc-bias voltages on the order of 12 V, much larger than normally permitted in standard integrated circuit (IC) technologies, have been required to attain GSM-compliant phase noise specifications [8]. For off-chip filter applications, impedance needs in the 50-377 Ω range (e.g., for antenna matching) are even more challenging, so require even higher voltages. Needless to say, a method for attaining low impedance with IC-amenable voltages would be highly desirable.

For this matter, micromechanical resonators using piezoelectric transducers already achieve low impedance, and without the need for bias voltages. Although many such piezoelectric designs suffer the drawback of having frequencies governed primarily by thickness, hence, not CAD definable; new piezoelectric micromechanical resonators that harness the d_{31} coefficient to allow lateral operation now circumvent this problem [9], making piezoelectric transduction much more attractive. Still, the (so far) higher

Q's of capacitively transduced resonators, their allowance for more flexible geometries with CAD-definable frequencies, plus their self-switching capability [10], voltage-controlled reconfigurability [11], better thermal stability [7], and material compatibility with integrated transistor circuits, make them sufficiently more attractive to justify intense research into methods for lowering their impedance while keeping voltages low. Among these, assuming that electrode-to-resonator gap spacings have already been minimized, methods that increase electrode-to-resonator overlap area by either direct geometrical modification [2][12][13] or mechanically-coupled arraying [14] have been most successful, albeit at the expense of die area.

This work lowers impedance while avoiding the need to increase the area of a capacitively transduced micromechanical resonator by raising the permittivity of the dielectric in its capacitive gap, thereby raising the efficiency of its transducer. Unlike the design of [15], which took a similar approach but used a vertical electrostatic force to effect a lateral displacement, with associated inefficiencies, the present approach directly applies a lateral force to effect a lateral displacement. This then allows the use of more general and higher *Q* resonator geometries, such as disk geometries. In this particular work, VHF and UHF MEMS-based vibrating micromechanical wine-glass mode disks [8] equipped with new solid dielectric-filled capacitive transducer gaps to replace previously used air gaps have been demonstrated at 160 MHz, with *Q*'s ~ 20,200 on par with those of air-gap resonators, and motional resistances (R_x's) more than 8× smaller at similar frequencies and bias conditions. This degree of motional resistance reduction comes about via not only the higher dielectric constant provided by a solid-filled electrode-to-resonator gap, but also by the ability to achieve smaller solid gaps than air gaps. These advantages with the right dielectric material may now allow capacitively-transduced resonators to match to the 50-377 Ω impedances expected by off-chip components (e.g., antennas) in many wireless applications without the need for high voltages. In addition, as will be seen, the use of filled-dielectric transducer gaps actually enhances the yield and reliability of capacitively transduced devices, since it removes problems generated by air gaps.

II. Air- vs. Solid-Gap Wine-Glass Disk Resonators

Again, this work uses disk resonator geometries operating in the compound (2,1)-mode (i.e., the "wine-glass disk" mode) to compare the performance of solid-gap versus air-gap capacitive transducers. Accordingly, some discussion of disk resonator fundamentals is in order, starting with that of previous air-gap versions.

A. Air Gap Wine-Glass Disk Resonator

Fig. 1(a) presents the perspective-view schematic of an air-gap wine-glass disk resonator, while Fig. 2 shows the electrical hookup required for two-port operation (in this case, using a solid-gap disk to be described later). As shown, the 60-MHz "wine-glass" device used here comprises a 32μm-radius, 3μm-thick disk supported by two beams that attach to the disk at its quasi-nodal points [8], where radial displacements are negligible compared to other parts of the disk structure when the disk vibrates in its wine-glass mode shape, shown in Fig. 3(a). In this mode shape, the disk expands along one axis and contracts in the orthogonal axis. Electrodes surround the disk with lateral electrode-to-disk air-gap spacings on the order of only 80 nm. To operate this device, a dc-bias V_P is applied to the disk structure, and an ac voltage v_i is applied to the input electrodes. (Note that there is no current flowing once the conductive structure is charged to V_P, so there is no dc power consumption). This $V_P v_i$ voltage combination generates a time-varying force proportional to the product $V_P v_i$ that drives the disk into the wine-glass mode shape when the frequency of v_i matches the wine-glass resonance frequency f_o, obtainable by solution of [16]

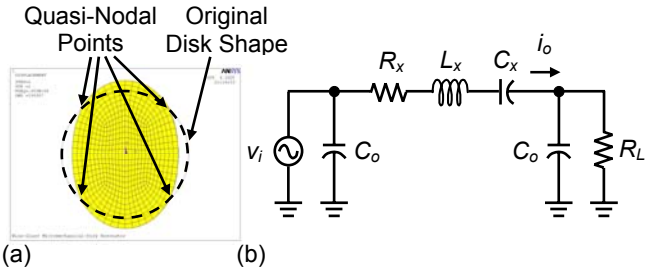

Fig. 3: (a) ANSYS mode-shape simulation and (b) electrical equivalent circuit for a wine-glass disk resonator.

$$\left[\Psi_n\left(\frac{\zeta}{\xi}\right)-n-q\right]\cdot\left[\Psi_n(\zeta)-n-q\right]=(nq-n)^2 \tag{1}$$

where

$$\Psi_n(x)=\frac{xJ_{n-1}(x)}{J_n(x)},\quad \zeta=2\pi f_o R\sqrt{\frac{\rho(2+2\sigma)}{E}}$$
$$\xi=\sqrt{\frac{2}{1-\sigma}},\quad q=\frac{\zeta^2}{2n^2-2},\quad n=2 \tag{2}$$

and where $J_n(x)$ is a Bessel function of the first kind of order n; the $\Psi_n(x)$ are modified quotients of $J_n(x)$; R is the disk radius; and ρ, σ, and E, are the density, Poisson ratio, and Young's modulus, respectively, of the disk structural material. Although hidden in the precision of (1)'s formulation, the resonance frequency f_o of this wine-glass disk is to first order inversely proportional to its radius R.

Once vibrating, the dc-biased (by V_P) time-varying output electrode-to-resonator capacitors generate output currents i_o equal to

$$i_o=V_P\cdot\frac{\partial C}{\partial r}\cdot\frac{\partial r}{\partial t}\cong V_P\cdot\left(\frac{\varepsilon_r\varepsilon_o A_o}{d_o^2}\right)\cdot(\omega_o X) \tag{3}$$

where A_o and d_o are the electrode-to-resonator overlap area and static gap spacing, respectively; ε_r is the permittivity in

the gap (in this case, of air, $\varepsilon_r = 1$); $\partial C/\partial r$ is the change in resonator-to-electrode capacitance per unit radial displacement; X is the amplitude of disk vibration; and $\omega_o = 2\pi f_o$ is the radian resonance frequency. Here, $\partial C/\partial r$ is approximated for simplicity, but a more complete formulation can be found in [8].

B. Series Motional Resistance, R_x

Fig. 3(b) presents the electrical equivalent circuit of the wine-glass disk resonator operated as a two-port (c.f., Fig. 2), where R_x, L_x, and C_x are its motional resistance, inductance, and capacitance, respectively; and C_o is the static electrode-to-disk capacitance. At resonance, L_x and C_x cancel, at which point the series motional resistance R_x of the resonator governs the relationship between v_i and i_o (i.e., governs the impedance), and is determined approximately by the expression

$$R_{x(\text{Air Gap})} = \frac{v_i}{i_o} \cong \frac{k_r}{\omega_o V_P^2} \cdot \frac{d_o^4}{\varepsilon_r^2 \varepsilon_o^2 A_o^2} \cdot \frac{1}{Q_{(\text{Air Gap})}} \tag{4}$$

where k_r is the effective stiffness of the resonator [8], and $\varepsilon_r = 1$ for air gap resonators.

From (4), R_x can be lowered by (a) raising the dc-bias voltage V_P; (b) scaling down the electrode-to-resonator gap d_o; (c) increasing the electrode-to-resonator overlap area A_o; and (d) increasing the permittivity ε_r of the electrode-to-resonator gap material. Of these approaches, lowering the gap spacing is by far the most effective, with a fourth power dependence. For air-gap resonators, however, the degree to which gap spacing can be lowered is limited by fabrication and linearity considerations, where too small a gap can compromise linearity and degrade the pull-in voltage to an unacceptably small value. The next most effective R_x-lowering parameters are the dc-bias voltage V_P, electrode-to-resonator overlap area A_o, and permittivity ε_r, all of which when increased reduce R_x by square law functions. The degree to which dc-bias voltage can be increased for an air-gap resonator is limited by either the pull-in voltage or by the maximum system supply voltage. The degree to which area can be increased is limited by the maximum acceptable die footprint for the resonator, which in turn is governed by cost. Before this work, permittivity was normally relegated to that of air or vacuum for lateral resonators, like the disk of this work. The next section now addresses the degree to which permittivity can be increased.

C. Solid Nitride Gap Wine-Glass Disk Resonator

Fig. 1(b) presents the perspective-view schematic of the solid-gap micromechanical wine-glass disk resonator used in this work. As shown, this device is identical to its air-gap counterpart except for its electrode-to-resonator gaps, which are now filled with a solid dielectric material (in this case, silicon nitride, with $\varepsilon_r = 7.8$). The presence of a dielectric in the gap actually provides a two-fold advantage in capacitive transducer efficiency (a) from the higher dielectric constant;

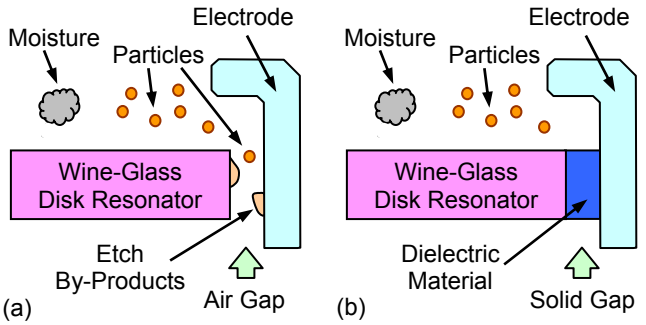

Fig. 4: Perspective view schematics of (a) an air gap and (b) a solid gap, illustrating how a solid gap can better avoid issues with moisture, particles, and undesired etch by-products.

and (b) by virtue of the fact that a smaller gap can now be achieved. The latter of these comes about because the gap no longer needs to be etched out, so is no longer limited by the ability of etchants to diffuse into the gap—something that has proved problematic in the past. In addition, the electrode and resonator can no longer be pulled into one another, so the catastrophic pull-in voltage is no longer an issue. (But read on for another voltage limitation due to dielectric breakdown.)

The above advantages, however, are somewhat dampened by the impedance of the solid dielectric material now in direct contact with the disk, replacing the low impedance air or vacuum present before. This solid material now imposes its own impedance into the system and can greatly reduce the overall displacement of the capacitive transducer electrodes, thereby reducing the output motional current. The expression for the output motional current of a solid-gap wine-glass mode disk resonator, of course, depends mainly on the compression and expansion of the solid-gap material, and is given by

$$i_o = V_P \cdot \frac{\partial C}{\partial r} \cdot \frac{\partial r}{\partial t} \cong V_P \cdot \left(\frac{\varepsilon_r \varepsilon_o A_o}{d_o^2} \right) \cdot (\omega_o X_N) \tag{5}$$

where X_N is the edge-to-edge displacement of the solid-gap mateiral, and $\varepsilon_r = 7.8$ for the case of the silicon nitride gap material used in this work.

The motional resistance of a solid-gap resonator can then be approximately expressed as

$$R_{x(\text{Solid Gap})} = \frac{v_i}{i_o} \cong \frac{k_r}{\omega_o V_P^2} \cdot \frac{d_o^4}{\varepsilon_r^2 \varepsilon_o^2 A_o^2} \cdot \frac{1}{Q_{(\text{Solid Gap})}} \cdot \frac{1}{\gamma} \tag{6}$$

where γ is a modified quotient of stiffness between the solid gap and surrounding electrode plates that at present is empirically extracted from measurement results. Dividing (6) by (4), the factor β by which use of a solid dielectric capacitive gap reduces the series motional resistance R_x can be expressed as

$$\beta = \frac{R_{x(\text{Air Gap})}}{R_{x(\text{Solid Gap})}} = \varepsilon_{r(\text{Solid Gap})}^2 \cdot \gamma \cdot \frac{Q_{(\text{Solid Gap})}}{Q_{(\text{Air Gap})}} \cdot \frac{d_{o(\text{Air Gap})}^4}{d_{o(\text{Solid Gap})}^4} \tag{7}$$

From (7), the factor by which R_x is reduced can be maximized by increasing the dielectric constant of the solid gap material, by reducing the electrode-to-resonator gap spacing (which, as already mentioned, is enabled via use of a solid gap), and by impedance matching the solid gap material to the resonator-electrode system so as to maximize the edge-to-edge displacement of the solid gap material X_N.

D. Additional Solid Gap Advantages

In addition to lower motional resistance, the use of solid dielectric-filled transducer gaps is expected to provide numerous other practical advantages over the air gap variety. In particular, the presence of a solid dielectric in the gap

1) better stabilizes the resonator structure against shock and microphonics;
2) eliminates the possibility of particles getting into an electrode-to-resonator air gap, which poses a potential reliability issue, as shown in Fig. 4;
3) greatly improves fabrication yield, by eliminating the difficult sacrificial release step needed for air gap devices; and
4) potentially allows larger micromechanical circuits (e.g., bandpass filters comprised of interlinked resonators) by stabilizing constituent resonators as the circuits they comprise grow in complexity.

In essence, the above advantages translate to lower overall manufacturing cost, since fewer devices are lost during the manufacturing process. This perhaps is an even more important benefit than motional resistance reduction.

E. Solid-Gap Design Issue: Increased Overlap Capacitance

In tandem with the advantages outlined above, solid gap resonators introduce design considerations that were not present for previous air gap resonators. Perhaps the most important of these arises from the much higher permittivity and smaller gap spacing they provide, which drive the static electrode-to-disk capacitance C_o, shown in Fig. 3(b) and given by

$$C_o = \frac{\varepsilon_r \varepsilon_o A_o}{d_o} = \frac{\varepsilon_r \varepsilon_o \pi R h}{d_o}, \qquad (8)$$

to much higher values than previous air gap counterparts. In particular, if when converting to a solid gap design, the electrode-to-resonator gap spacing d_o decreases from 80 nm to 20 nm, and ε_r increases from 1 to 7.8, C_o becomes 31.2× larger. At first, this seems to be a significant problem, since this larger C_o would increase capacitive loading, making circuit design at high frequency more difficult. However, note that R_x is a stronger function of d_o and ε_r than C_o, so it shrinks faster than C_o grows, actually making circuit and system design easier (in most cases) when using solid-gap resonators.

III. Fabrication

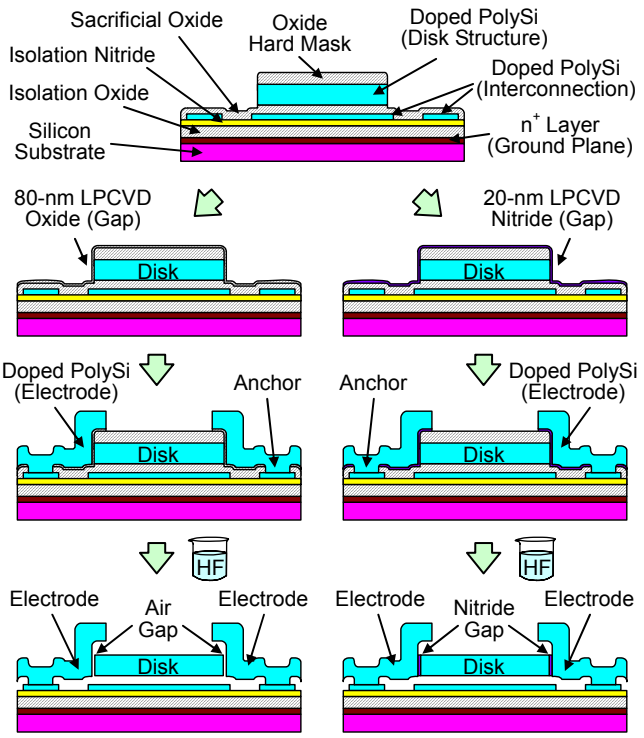

Fig. 5: Cross-section views briefly describing the fabrication processes used for air-gap (left fork) and solid-gap (right fork) wine-glass disk resonators.

The micromechanical wine-glass disk resonators measured in this work were fabricated via processes based upon the self-aligned, small lateral gap, polysilicon wafer-level surface-micromachining process previously used to achieve GHz disk resonators in [3]. In this process, summarized by the left fork in Fig. 5, lateral electrode-to-resonator air-gap spacings are defined by the thickness of a conformally deposited sidewall oxide layer, which is later removed by an isotropic hydrofluoric acid (HF) wet etchant to achieve the desired electrode-to-resonator air gaps. The air-gap resonators of this work used this exact process.

For solid-gap resonators, the process in the right fork of Fig. 5 was used, where silicon nitride, instead of silicon dioxide, is deposited via LPCVD to form the sidewall spacer. During the sacrificial hydrofluoric acid release step, the oxide underneath and above the disk-electrode structure is removed, as is any exposed nitride (due to the finite 10 nm/min etch rate of nitride in HF), but the nitride in the electrode-to-resonator gap remains intact, since it is effectively protected from HF attack by the slow diffusion of the wet etchant into the tiny solid nitride-filled electrode-to-resonator gap. Interestingly, the air-gap process actually proved to be the more difficult of the two, because it required removal of oxide in small gaps, which is a difficult, diffusion-limited process. As a consequence, the solid-gap designs were able to achieve smaller gaps of 20 nm, whereas the air gaps were limited to about 60 nm.

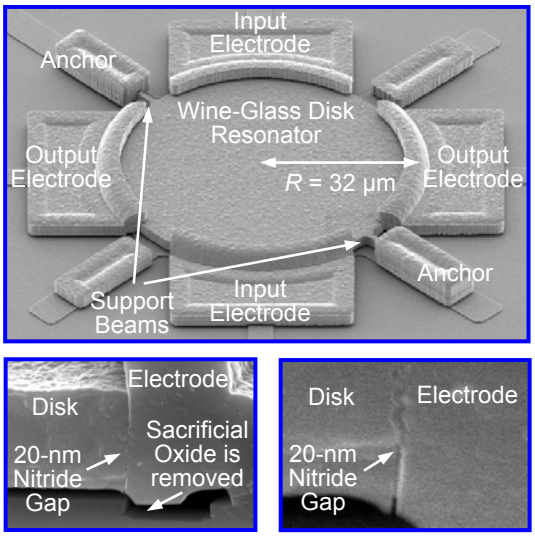

Fig. 6: SEM's of a fabricated 60-MHz wine-glass disk resonator with solid nitride gap. The bottom two SEM's zoom in on the 20-nm solid gaps.

Fig. 6 presents the SEM of a fabricated 60-MHz micro-mechanical wine-glass disk resonator, together with two zoom-in views of its 20-nm solid nitride gap. As shown, even after a 35 minute long hydrofluoric acid release etch, only a negligible amount of nitride at the top and bottom edges is removed, and most of the nitride is still left in the gap.

IV. Experimental Results

Wine-glass disk resonators equipped with 80-nm air and 20-nm nitride gaps were tested inside a custom-built chamber capable of reaching vacuums down to 50 μTorr. The chamber had electrical feedthroughs that connected a pc board housing resonator dies to external measurement instrumentation, all interconnected as in the two-port setup of Fig. 2.

Interestingly, the maximum usable dc-bias in this setup was not governed by the pull-in voltage of the air-gap disks, but rather by the breakdown voltage of their nitride-gap counterparts, which ended up being only 12 V for the 20-nm nitride gap devices used here. As expected, the breakdown voltage was a function of nitride filler quality, and varied from 4 V to 12 V, depending upon the quality of nitride sidewall deposition. The 12 V value is consistent with the 6-10 MV/cm dielectric breakdown electric field for nitride. It should be noted that 12 V is not that much smaller than the 15 V pull-in voltage typical for an 80-nm air-gap disk. Further, if a 20-nm air-gap could be achieved (i.e., could be cleared in a release step), then the pull-in voltage for the associated disk would likely be lower than the 12 V breakdown of a 20-nm nitride gap. In other words, a solid nitride gap likely allows a higher dc-bias voltage than an equivalent air gap.

To stay clear of solid-dielectric breakdown, measurement

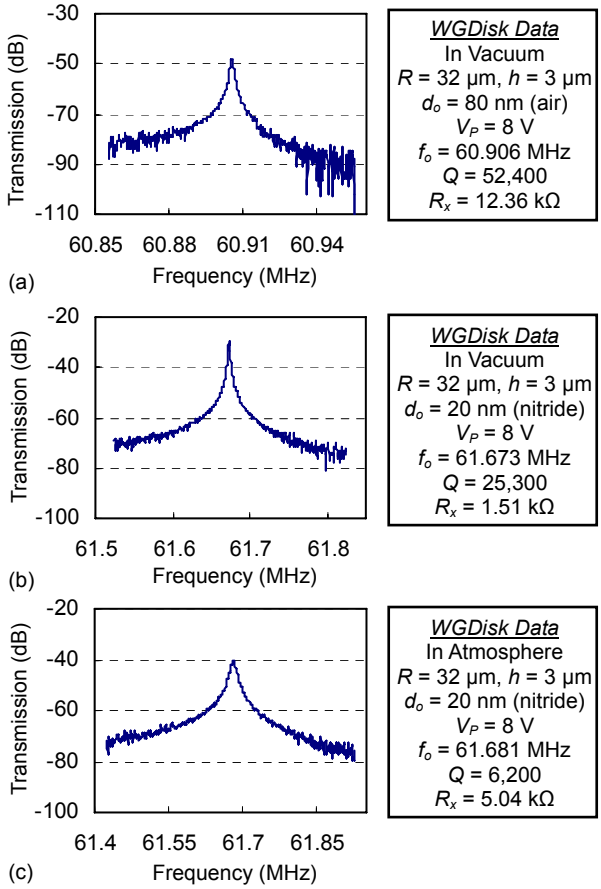

Fig. 7: Measured frequency characteristic for a fabricated 60-MHz wine-glass disk resonator with (a) 80-nm air gap tested in vacuum (b) 20-nm nitride gap tested in vacuum, and (c) 20-nm nitride gap tested in atmosphere.

dc-bias voltages for 60-MHz disks were constrained to only 8 V. Fig. 7(a) and Fig. 7(b) present measured frequency characteristics using the setup of Fig. 2 under 50 μTorr vacuum for 60-MHz wine-glass disk resonators with 80-nm air-gap and 20-nm nitride-gap capacitive transducers, respectively. As shown, compared with the 60.906 MHz and $Q = 52{,}400$ of its air-gap counterpart, the nitride-gap wine-glass disk resonator not only retained a very similar resonance frequency of 61.673 MHz, only 1.26% different; but also exhibited a Q of 25,300, which is about half that of the air gap device, but still more than adequate for the most demanding communications applications; and all while achieving an 8.19× smaller R_x down to only 1.51 kΩ, verifying the expectations of Section II. If a larger dc-bias bias voltage were permitted, perhaps by improving the quality of the gap-filling nitride dielectric material, even smaller values of R_x should be achievable.

Interestingly, filling the electrode-to-resonator gap with a solid does not seem to impact the Q a great deal. It does, however, greatly reduce the plate-to-plate displacement in the capacitive transducer. In particular, the measured output

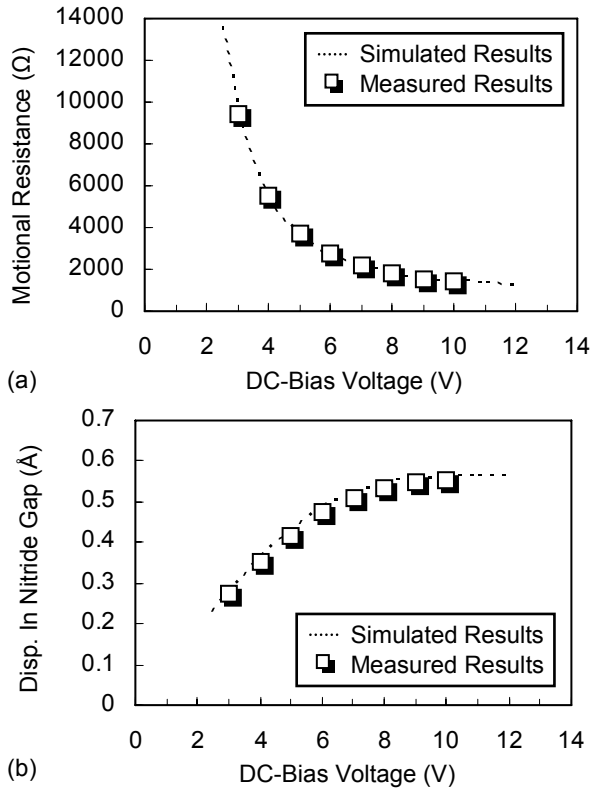

Fig. 8: Measured and predicted (a) motional resistance and (b) edge-to-edge nitride gap displacement versus dc-bias voltage, respectively, for a 60-MHz wine-glass disk resonator with 20-nm nitride gap.

motional current of 5.5 μA corresponds to a peak gap thickness displacement of only 0.53 Å for the solid-gap wine-glass disk, to be compared with the ~20 Å of its air-gap counterpart. To further explore the degree of reduction in edge-to-edge gap displacement, Fig. 8(a) and Fig. 8(b) present measured and simulated (using the formulation of Section II) motional resistance and nitride displacement versus dc-bias voltage, respectively, for a 60-MHz wine-glass disk resonator with a 20-nm nitride electrode-to-resonator gap. As shown, the measured results match well with the predicted results from (6), where a stiffness quotient γ of 7.67×10^{-4} is extracted from one of the data points. Despite the reduction in plate-to-plate displacement, the increase in dielectric permittivity and smaller 20-nm gap afforded via use of a solid nitride gap still insure a sizable net reduction in R_x.

To compare vacuum versus air operation of solid-gap micromechanical disks, Fig. 7(c) presents measured frequency response spectra for the same 60-MHz nitride gap wine-glass disk resonator shown in Fig. 7(b), but in atmosphere rather than in vacuum. As shown, the measured Q of 6,200 in atmosphere, while still very good, is much smaller than the Q of 25,300 it posts in vacuum—a result that poses somewhat of a quandary, since a solid gap should not pump gas the way that an air-gap would, so should suffer much

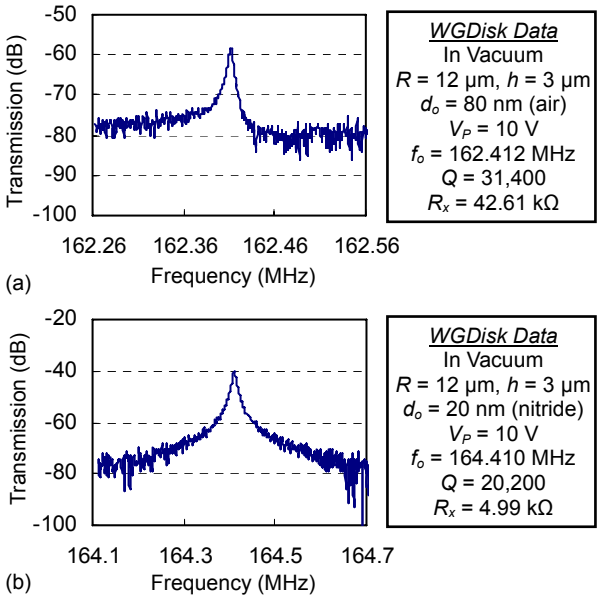

Fig. 9: Measured frequency characteristic for a fabricated 160-MHz wine-glass disk resonator with (a) 80-nm air gap tested in vacuum and (b) 20-nm nitride gap tested in vacuum.

less Q degradation when switching from vacuum to air. The fact that Q does degrade significantly might indicate either (a) the electrodes are moving in unison with the disk itself, pushing air around, while the nitride gap compresses ever so slightly (i.e., only 0.53 Å); (b) the solid nitride gap is not solidly attached to either the disk or electrode, allowing a very small amount of movement across a tiny 0.53 Å air gap, which pumps air, thereby lowering Q; or (c) the nitride material in the gap is porous, with air bubbles, that get pumped as the gap compresses and expands. Unfortunately, the zoom-in SEM's of Fig. 6 are not clear enough to definitively tell which of the above is true, so more investigation into this is needed, and is the subject of future work.

In the meantime, measurements were taken to verify the efficacy of solid-gap design at even higher frequencies. Fig. 9(a) and Fig. 9(b) present measured frequency characteristics under 50 μTorr vacuum for 160-MHz wine-glass disk resonators with 80-nm air and 20-nm nitride gaps, respectively. Again, the nitride gap resonator has similar a resonance frequency, a slightly smaller but still impressive Q of 20,200, and an 8.54× smaller R_x, compared to its air gap counterpart.

V. Towards Even Lower Impedance

The 8× reduction in series motional resistance demonstrated using solid-nitride capacitive transducer gaps in this work, although already impressive, is only an inkling of what should be possible. Indeed, there are many other thin-film dielectrics with much higher dielectric constants than silicon nitride, including hafnium dioxide (HfO_2,

$\varepsilon_r = 25$), titanium dioxide (TiO_2, $\varepsilon_r = 80$), or barium strontium titanate (BST, $Ba_xSr_{1-x}TiO_3$, $\varepsilon_r \sim 300$). With an inverse square law dependence of R_x on permittivity, there seems to be plenty of room for further impedance improvement. Fig. 10 plots predicted values of series motional resistance R_x (using the theory of Section II, together with the conservative, empirically determined γ) versus dc-bias voltage V_P, showing that impedances on the order of 50 Ω might be achievable with IC-compatible dc-bias voltages of only 0.91 V. Work pursuant to this goal is presently underway.

VI. Conclusions

MEMS-based vibrating micromechanical resonators equipped with solid dielectric lateral capacitive transducer gaps have been demonstrated for the first time. Compared to otherwise identical air gap versions, solid gap resonators have similar resonant frequencies, slightly smaller, but still very impressive high Q's, and much smaller motional resistance. Viewed from the perspective of dc-bias voltage, the same impedance can be achieved in a solid gap resonator as an air gap counterpart, but using a much smaller dc-bias voltage—a very important feature that should greatly simplify future integration of MEMS resonators with integrated circuit transistors. In addition to lower motional resistance, solid gap resonators provide many other advantages over the air gap variety, such as better stabilization, better resilience against shock, better reliability, and better fabrication yield.

Acknowledgment: This work is supported under DARPA Grant No. F30602-01-1-0573.

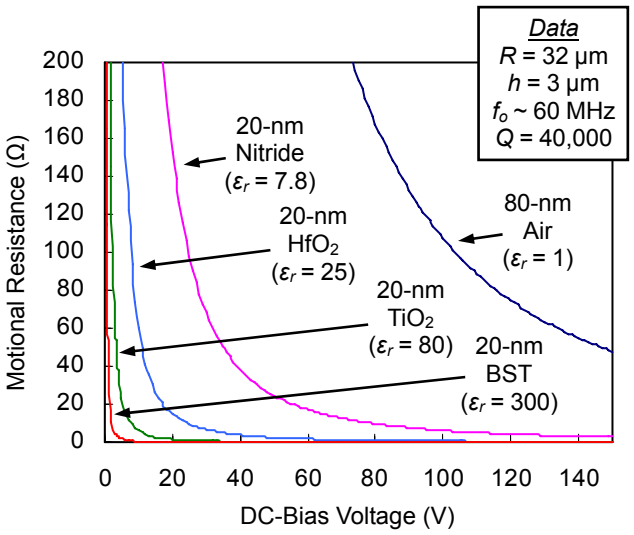

Fig. 10: Predicted values of motional resistance versus dc-bias voltage for different dielectric materials.

References:

[1] J. Wang, J. E. Butler, T. Feygelson, and C. T.-C. Nguyen, "1.51-GHz polydiamond micromechanical disk resonator with impedance-mismatched isolating support," *Technical Digest*, IEEE Int. Micro Electro Mechanical Systems Conf., Maastricht, The Netherlands, Jan. 2004, pp. 641-644.

[2] S.-S. Li, Y.-W. Lin, Y. Xie, Z. Ren, and C. T.-C. Nguyen, "Micromechanical "hollow-disk" ring resonators," *Technical Digest*, IEEE Int. Micro Electro Mechanical Systems Conf., Maastricht, The Netherlands, Jan. 2004, pp. 821-824.

[3] J. Wang, Z. Ren, and C. T.-C. Nguyen, "1.156-GHz self-aligned vibrating micromechanical disk resonator," *IEEE Transactions on Ultrasonics, Ferroelectrics, and Frequency Control*, vol. 51, no. 12, pp. 1607-1628, Dec. 2004.

[4] C. T.-C. Nguyen, "Vibrating RF MEMS for next generation wireless applications," *Proceedings*, IEEE Custom Integrated Circuits Conf., Orlando, FL, Oct. 2004, pp. 257-264.

[5] V. Kaajakari, J. Kiihamäki, A. Oja, H. Seppä, S. Pietikäinen, V. Kokkala, and H. Kuisma, "Stability of wafer level vacuum encapsulated single-crystal silicon resonators," *Digest of Technical Papers,* Int. Conf. on Solid-State Sensors, Actuators, and Microsystems (Transducers'05), Seoul, Korea, June 2005, pp. 916-919.

[6] B. Kim, R. N. Candler, M. Hopcroft, M. Agarwal, W.-T. Park, and T. W. Kenny, "Frequency stability of wafer-scale encapsulated MEMS resonators," *Digest of Technical Papers,* Int. Conf. on Solid-State Sensors, Actuators, and Microsystems (Transducers'05), Seoul, Korea, June 2005, pp. 1965-1968.

[7] W.-T. Hsu and C. T.-C. Nguyen, "Stiffness-compensated temperature-insensitive micromechanical resonators," *Technical Digest*, IEEE Int. Micro Electro Mechanical Systems Conf., Las Vegas, NV, Jan. 2002, pp. 731-734.

[8] Y.-W. Lin, S. Lee, S.-S. Li, Y. Xie, Z. Ren, and C. T.-C. Nguyen, "Series-resonant VHF micromechanical resonator reference oscillators," *IEEE Journal of Solid-State Circuits*, vol. 39, no. 12, pp. 2477-2491, Dec. 2004.

[9] G. Piazza, P. J. Stephanou, J. M. Porter, M. B. J. Wijesundara, and A. P. Pisano, "Low motional resistance ring-shaped contour-mode aluminum nitride piezoelectric micromechanical resonators for UHF applications," *Technical Digest*, IEEE Int. Micro Electro Mechanical Systems Conf., Miami Beach, FL, Jan. 2005, pp. 20-23.

[10] S.-S. Li, Y.-W. Lin, Z. Ren, and C. T.-C. Nguyen, "Self-switching vibrating micromechanical filter bank," *Proceedings*, IEEE Joint Int. Frequency Control / Precision Time & Time Interval Symposium, Vancouver, Canada, Aug. 2005, to be published.

[11] A.-C. Wong and C. T.-C. Nguyen, "Micromechanical mixer-filters ("Mixlers")," *Journal of Microelectromechanical Systems*, vol. 13, no. 1, pp. 100-112, Feb. 2004.

[12] B. Bircumshaw, G. Liu, H. Takeuchi, T.-J. King, R. Howe, O. O'Reilly, and A. Pisano, "The radial bulk annular resonator: towards a 50Ω RF MEMS filter," *Digest of Technical Papers*, Int. Conf. on Solid-State Sensors, Actuators, and Microsystems (Transducers'03), Boston, MA, June 2003, pp. 875-878.

[13] Y. Xie, S.-S. Li, Y.-W. Lin, Z. Ren, and C. T.-C. Nguyen, "UHF micromechanical extensional wine-glass mode ring resonators," *Technical Digest*, IEEE International Electron Devices Meeting, Washington DC, WA, Dec. 2003, pp. 953-956.

[14] M. U. Demirci, M. A. Abdelmoneum, and C. T.-C. Nguyen, "Mechanically corner-coupled square microresonator array for reduced series motional resistance," *Digest of Technical Papers*, Int. Conf. on Solid-State Sensors, Actuators, and Microsystems (Transducers'03), Boston, MA, June 2003, pp. 955-958.

[15] S. A. Bhave and R. T. Howe, "Silicon nitride-on-silicon bar resonator using internal electrostatic transduction," *Digest of Technical Papers,* Int. Conf. on Solid-State Sensors, Actuators, and Microsystems (Transducers'05), Seoul, Korea, June 2005, pp. 2139-2142.

[16] M. Onoe, "Contour vibrations of isotropic circular plates," *J. Acoustical Society of America*, vol. 28, no. 6, pp. 1158-1162, Nov. 1956.